# Axial dispersion of Brownian colloids in microfluidic channels

Michael P. Howard,[1] Aishwarya Gautam,[1]
Athanassios Z. Panagiotopoulos,[1] and Arash Nikoubashman[2,*]
[1]*Department of Chemical and Biological Engineering, Princeton University, Princeton, New Jersey 08544, USA*
[2]*Institute of Physics, Johannes Gutenberg University Mainz, Staudingerweg 7, 55128 Mainz, Germany*
(Received 29 April 2016; published 19 August 2016)

We present a complete theoretical framework for the axial dispersion of a Brownian colloidal suspension confined in a parallel plate channel, extending the Taylor-Aris treatment to particles with diameters comparable to the channel width. The theoretical model incorporates the effects of confinement on the colloid distribution, corrections to the velocity profile due to the effects of colloid concentration on the suspension viscosity, and position-dependent diffusivities. We test the theoretical model using explicit-solvent molecular dynamics simulations that fully incorporate hydrodynamic correlations and thermal fluctuations and obtain good quantitative agreement between theory and simulations. We find that the nonuniform colloid distributions that arise in confinement due to excluded volume between the colloids and channel walls significantly impact the axial dispersion.

DOI: 10.1103/PhysRevFluids.1.044203

## I. INTRODUCTION

Particles in nonuniform flow fields undergo an enhanced axial dispersion (spreading) compared to diffusion in the absence of flow [1]. Qualitatively, axial dispersion is enhanced by flow because particles diffuse across streamlines and advect at rates different from the average velocity, resulting in a net spreading relative to the mean. In his seminal papers [2,3], Taylor calculated the asymptotic form of this dispersion coefficient for noninteracting pointlike tracer particles in a cylindrical tube under the assumptions that the solute particles diffuse isotropically and explore all streamlines of the flow field uniformly. Aris subsequently performed a moment analysis that justified the assumptions in Taylor's original analysis and captured the transient evolution of the dispersion [4].

The Taylor-Aris description of dispersion works well for molecular solutions, whose components are considerably smaller than the channel diameter. However, the physical picture becomes significantly more complicated for colloidal systems. Some volume of the channel is excluded to the colloids due to their finite diameters. Under sufficient confinement, the excluded volume between the colloids and channel walls can establish a nonuniform colloid distribution [5–7]. This means that the colloids do not explore all streamlines equally. Moreover, due to hydrodynamic interactions between the colloids and the channel walls, the colloid diffusion tensor can be anisotropic [8]; the diffusion coefficient normal to the channel walls may differ significantly from the axial diffusion coefficient even at rest. For sufficiently high colloid concentrations, secondary flows between colloids may also modify the effective flow field or diffusion coefficient.

Brenner and Gaydos have comprehensively treated the dispersion problem for a single colloid in a cylindrical pore [9]. Their theory accounts for anisotropic diffusion and an applied external field on the colloid. Silebi and DosRamos applied DLVO theory (named after Derjaguin, Landau, Verwey and Overbeek) to compute the forces between colloids and the walls of a capillary tube and also accounted for an effective external potential due to inertial lift on the colloids [10]. A simplified version of the Brenner and Gaydos theory, assuming no external field and isotropic diffusion, has

*anikouba@uni-mainz.de

 

also been developed for rigid colloids between parallel plates and amounts to the introduction of an additional geometric factor that reduces the actual dispersion from the Taylor-Aris value [11]. Bhattacharya *et al.* applied a perturbation method to analyze the dispersion of finite-size particles confined in cylindrical tubes subject to inertial lift [12]. However, these theories do not account for nonuniform colloid distributions that can arise even when the colloids have only hard-core volume exclusion with the channel walls. Moreover, classical dispersion theory results may not be sufficiently accurate to model dispersion in a confined suspension, where hydrodynamic coupling between many colloids and the channel walls can affect the dispersion. For example, Griffiths and Stone showed that shear-enhanced diffusion can cause a reduction of the axial dispersion [13].

The invention of microfluidic devices has fueled interest in Taylor-Aris dispersion in order to control dispersion [14–16], improve micromixing [17,18], probe flow fields [19], and measure colloid [20] and nanoparticle [21] diffusion coefficients. Unfortunately, experimental validation of theoretical models for axial dispersion remains challenging due to the small diffusion coefficients of the colloids, which necessitate long channels for capturing the long-time dispersion [22], and the difficulty of performing particle-tracking measurements with sufficient spatial and temporal resolution. Computer simulations are an ideal tool to address these issues because they allow for the precise tracking of the colloidal particles, direct measurement of the flow fields, and systematic control over the relevant parameters, such as solute concentration and flow strength. Recently, two-dimensional mesoscale simulations were performed to study the axial dispersion of repulsive colloidal disks of varying diameter [23]. Significant deviations from the theoretical Taylor-Aris prediction were observed, but due to the challenge of obtaining reliable statistics the authors were unable to conclude whether existing theory was sufficient to describe this behavior.

In this contribution, we develop a theory for the axial dispersion of dilute Brownian colloids in a parallel plate geometry that explicitly takes into account the effects of colloid concentration and confinement on the colloid distribution, velocity profile, and diffusion coefficients. We describe a framework to estimate all of the necessary parameters to reliably predict the enhancement to the axial dispersion. We perform complementary molecular dynamics simulations to directly test our theoretical predictions. Our simulation approach fully takes into account hydrodynamic interactions and thermal fluctuations.

The article is organized as follows. In Sec. II, we derive an expression for the axial dispersion of colloids in the parallel plate geometry. We introduce our simulation model and methodology in Sec. III. We present our results and findings in Sec. IV, and provide a brief summary and outlook in Sec. V.

## II. THEORY

The analysis presented by Brenner and Gaydos [9] for a colloidal particle in a cylindrical pore can be straightforwardly applied to the parallel plate geometry, schematically drawn in Fig. 1. The coordinate system has been chosen so that the principal axes coincide with the transverse ($x$),

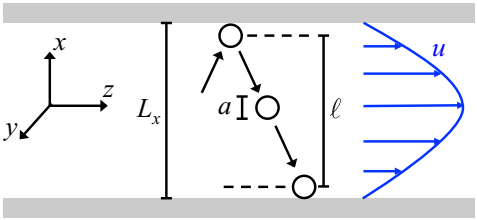


FIG. 1. Schematic representation of flow in the parallel plate geometry, indicating the transverse ($x$), vorticity ($y$), and axial ($z$) directions. The colloid of diameter $a$ diffuses in the accessible width $\ell$ of the full channel width $L_x$, and is advected by the velocity field $u$.

vorticity ($y$), and axial directions ($z$). Due to the channel walls, the colloid center of mass cannot cross the boundaries at $x = \pm\ell/2$. The accessible width $\ell$ will be smaller than the actual channel width $L_x$ because of the finite particle diameter $a$.

We model the time-dependent probability distribution $p$ for the center-of-mass position of a single colloid. In doing so, we neglect correlations between the distributions of different particles and assume that the colloid has negligible inertia on the time scales of interest so that its velocity is Maxwell-Boltzmann distributed. Then, the time evolution of the distribution is governed by the Smoluchowski equation,

$$\frac{\partial p}{\partial t} + \nabla \cdot \mathbf{j} = 0, \tag{1}$$

with a probability flux $\mathbf{j}$,

$$\mathbf{j} = p\mathbf{u} - \mathbf{D} \cdot \nabla p - p\beta \mathbf{D} \cdot \nabla \phi. \tag{2}$$

The first term is the advection due to the flow field $\mathbf{u}$, the second term is the diffusion due to Brownian motion with diffusion tensor $\mathbf{D}$, and the third term represents an applied force due to some external potential $\phi$, where $\beta = 1/(k_B T)$ is the inverse temperature.

Concentration and confinement effects of the suspension are included in a mean-field treatment through the effective flow field, diffusivity, and external potential. In the parallel plate geometry, the flow field is expected to be one dimensional in nature: $\mathbf{u} = u(x)\mathbf{e}_z$. Moreover, in the absence of an applied field, the external potential should only be due to the effects of confinement between the walls so that $\phi = \phi(x)$. We neglect any shear-enhanced diffusion so that $\mathbf{D}$ has only diagonal elements. This is justified for sufficiently small particles, low concentrations, or slow flow rates, where Brownian motion dominates over advective transport. Simplifying and applying a product rule to Eq. (2) yields the governing equation

$$\frac{\partial p}{\partial t} + u(x)\frac{\partial p}{\partial z} = \frac{\partial}{\partial x}\left\{ w(x) D_x(x) \frac{\partial}{\partial x}\left[ \frac{p}{w(x)} \right] \right\} + D_z(x)\frac{\partial^2 p}{\partial z^2}, \tag{3}$$

where $D_x$ is the diffusion coefficient in the transverse direction, $D_z$ is the diffusion coefficient in the axial direction, and $w$ is the normalized Boltzmann weight for the particle

$$w(x) = \frac{e^{-\beta\phi(x)}}{\int_{-\ell/2}^{\ell/2} e^{-\beta\phi(x)} dx}. \tag{4}$$

In order to close the problem, we apply no-flux boundary conditions at the walls, $\mathbf{j}_x(x = \pm\ell/2, z, t) = 0$, and assume an infinite channel in order to neglect entrance effects, $p(x, z \to \pm\infty, t) \to 0$. The colloid's initial position is assumed to be $(x_0, z_0)$, so $p(x, z, t = 0) = \delta(x - x_0)\delta(z - z_0)$ to make $p$ properly normalized. Under these conditions, it can be shown that $w$ is the steady-state marginal probability distribution for the colloid across $x$ (see the Appendix). In Eq. (3), we have assumed that $D_z$ is independent of the colloid's $z$ position, which is reasonable for an infinite channel. However, hydrodynamic interactions with the channel walls significantly influence diffusion as a function of transverse position [8], and so $D_x$ and $D_z$ are taken to be functions of $x$.

We seek the long-time dispersivity $K$ that quantifies the average spreading of the particle distribution, which is expected to have a contribution due to Brownian motion and an enhancement due to flow. We define $K$ using the Einstein relation for a Brownian particle in a moving frame of reference

$$K = \frac{1}{2} \lim_{t \to \infty} \frac{d}{dt} \langle (z - \langle z \rangle)^2 \rangle, \tag{5}$$

where the brackets indicate the total expectation taken using $p(x, z, t)$. Performing a moment analysis in the spirit of Aris [4] and Brenner and Gaydos [9] (see the Appendix for details) yields the

dispersivity

$$K = \overline{D}_z + \int_{-\ell/2}^{\ell/2} \frac{dx}{w(x)D_x(x)} \left\{ \int_{-\ell/2}^{x} [u(\hat{x}) - \overline{u}] w(\hat{x}) d\hat{x} \right\}^2, \tag{6}$$

where $\overline{D}_z$ is the average axial diffusion coefficient

$$\overline{D}_z = \int_{-\ell/2}^{\ell/2} D_z(x) w(x) dx, \tag{7}$$

and $\overline{u}$ is the mean velocity experienced by the colloid

$$\overline{u} = \int_{-\ell/2}^{\ell/2} u(x) w(x) dx. \tag{8}$$

The dispersivity $K$ is then fully determined by knowledge of only a few important parameters: (1) the steady-state colloid distribution $w$, (2) the velocity profile $u$, and (3) the diffusion tensor $\mathbf{D}$. Theoretical methods for estimating these parameters will be discussed in detail in Sec. IV.

## III. SIMULATION MODEL AND METHODS

In order to test the theoretical prediction of Eq. (6), we performed molecular dynamics (MD) simulations of colloidal suspensions under flow. Explicit-solvent molecular dynamics incorporates hydrodynamic effects, energetic interactions between particles, and thermal fluctuations. The solvent and colloids were modeled as spherical particles interacting through the Lennard-Jones potential

$$U_{ij}(r) = 4\varepsilon_{ij} \left[ \left( \frac{\sigma_{ij}}{r} \right)^{12} - \left( \frac{\sigma_{ij}}{r} \right)^{6} \right], \tag{9}$$

where $r$ is the distance between particles of types $i$ and $j$, $\varepsilon_{ij}$ sets the interaction strength, and $\sigma_{ij}$ sets the range of the interaction. Unless stated otherwise, the potential was truncated at $r_{\text{cut}} = 3\,\sigma_{ij}$ with a smoothing polynomial applied from $2.5\,\sigma_{ij}$ so that both the energy and force were zero at $r_{\text{cut}}$. In what follows, all quantities are reported in reduced units derived using the solvent-solvent interaction energy scale, $\varepsilon_{\text{ss}} = 1$; solvent-solvent interaction length scale, $\sigma_{\text{ss}} = 1$; and solvent particle mass, $m_{\text{s}} = 1$, as the fundamental units. For example, the derived unit of time is $\sqrt{m_{\text{s}}\sigma_{\text{ss}}^2/\varepsilon_{\text{ss}}}$ in this system of units.

Neutrally buoyant colloids were density matched to the solvent by setting their mass $m_{\text{c}} = \pi\rho_{\text{s}}a^3/6$, where $\rho_{\text{s}}$ is the solvent density and $a$ is the effective diameter of the colloids (see Sec. IV A). The interactions between colloids were modeled through the purely repulsive Weeks-Chandler-Anderson (WCA) potential [24], which is obtained by truncating Eq. (9) at its minimum, $r_{\text{cut}} = 2^{1/6}\,\sigma_{ij}$, and shifting it by $\varepsilon_{ij}$. The colloid-colloid interaction length was set to $\sigma_{\text{cc}} = 3$, and the interaction strength was set to $\varepsilon_{\text{cc}} = 10$ to reduce possible overlap between colloids. Colloid-solvent cross interactions were modeled using the Lennard-Jones potential with $\sigma_{\text{cs}} = (\sigma_{\text{cc}} + \sigma_{\text{ss}})/2 = 2$ and $\varepsilon_{\text{cs}} = 1$.

We confined our colloidal suspension between two planar walls in the $xy$ plane using a similar model to that of Khare and coworkers [25,26]. The walls were constructed by placing particles into one layer of a face-centered cubic crystal with lattice spacing 1.3 at $x = \pm 12$ and fixing their positions with stiff harmonic springs (spring constant 500). Wall particles interacted with each other through the Lennard-Jones potential with $\sigma_{\text{ww}} = 1$ and $\varepsilon_{\text{ww}} = 1$. Wall-solvent interactions were similarly treated with $\sigma_{\text{sw}} = 1$ and $\varepsilon_{\text{sw}} = 1$. The cross interactions with the colloid were modeled using the WCA potential with $\sigma_{\text{cw}} = 2$ and $\epsilon_{\text{cw}} = 1$. With this choice of parameters, the lattice spacing gave a nearest-neighbor distance smaller than $\sigma_{\text{ww}}$, which achieved two important effects: (1) the suspension could not penetrate the walls and (2) the walls became microscopically rough,

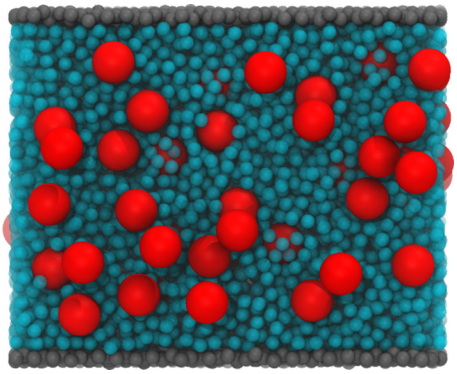

FIG. 2. Simulation snapshot [27] of the parallel plate channel for colloid volume fraction $\Phi = 0.1$. The coordinate axis is oriented as in Fig. 1.

which is essential to establish no-slip boundary conditions. A representative simulation snapshot is shown in Fig. 2.

Despite the purely repulsive colloid-wall interactions, we observed that the colloids would sometimes seem to stick to the channel walls, which limited our ability to statistically sample the entire colloid distribution during the accessible simulation time. We attribute this effect to structuring of the Lennard-Jones solvent and depletion forces that resulted in a weak net attraction of the colloids to the walls. In a physical suspension, there may be additional repulsive forces between the channel walls and the colloids, e.g., electrostatics, which counteract these attractions. The proposed theory is general and is able to accommodate such repulsive external fields imposed on the colloids. Accordingly, we introduced an additional purely repulsive potential acting only on the colloids

$$U_{\mathrm{r}}(x) = \varepsilon_{\mathrm{r}}\left[\frac{2}{15}\left(\frac{1}{|x - x_{\mathrm{r}}|}\right)^{9} - \left(\frac{1}{|x - x_{\mathrm{r}}|}\right)^{3}\right], \tag{10}$$

where $x$ is the transverse position of the colloid, $\varepsilon_{\mathrm{r}} = 144$ is the interaction strength, and the walls have been placed at $x_{\mathrm{r}} = \pm 10$. The potential was truncated at its minimum, $x_{\mathrm{cut}} = (2/5)^{1/6}$, and shifted by $\varepsilon_{\mathrm{r}}\sqrt{10}/3$. This potential effectively reduced the width of the channel that the colloid could explore by about 10%. We emphasize that this potential has been chosen as a matter of simulation convenience, and other wall interactions (including attractive surfaces) can also be incorporated into the theory through $\phi$ in Eq. (4).

We performed molecular dynamics simulations using the HOOMD-blue simulation package [28–30] with double precision floating point operations to minimize momentum drift during long simulations. The equations of motion were integrated using the velocity Verlet algorithm with a time step $\Delta t = 0.0025$. Due to the size asymmetry between the colloid and solvent particles, the pair force calculations were accelerated with a binary tree neighbor search [31]. Pressure-driven flow was generated by applying a constant gravitational body force $F_g = m_i g$ to all particles in the dispersion along the flow direction with acceleration constant $g$. The nonequilibrium flow of the suspension generates heat that must be dissipated to maintain the fluid at a constant temperature. In order to minimally perturb the dynamics of the suspension, a Langevin thermostat was applied to the wall particles with friction factor $\gamma = 4$, essentially turning the walls into heat sinks. The suspension was not explicitly thermostatted. All values of $g$ investigated in this work were sufficiently small so that the excess heat was efficiently dissipated through the walls and the system remained at the targeted temperature $T = 2.5$.

The suspensions were initialized by placing the colloid and solvent particles randomly on a lattice between the parallel plates in order to give a suspension density of approximately $\rho = 0.62$. We applied periodic boundary conditions in the vorticity ($y$) and axial ($z$) dimensions of our simulations

TABLE I. Number of colloids, $N_c$, and solvent particles, $N_s$, in the channel for targeted volume fraction, $\Phi$, and suspension density $\rho = 0.62$. $D$ is the simulated bulk diffusion coefficient of the suspension extrapolated to infinite box size. $\overline{D}_z$ is the simulated axial diffusion coefficient at rest in the parallel plate channel. Subscripts on reported values indicate the measurement uncertainty in the last digit.

| $\Phi$ | $N_c$ | $N_s$ | $D$ | $\overline{D}_z$ |
|---|---|---|---|---|
| 0.005 | 6 | 12822 | $0.126_1$ | $0.116_1$ |
| 0.025 | 30 | 12619 | $0.117_0$ | $0.107_1$ |
| 0.050 | 61 | 12356 | $0.110_0$ | $0.097_1$ |
| 0.075 | 91 | 12101 | $0.103_0$ | $0.089_0$ |
| 0.10 | 122 | 11838 | $0.096_0$ | $0.083_1$ |

with box lengths $L_y = L_z = 29.9$. This kept the suspensions at one effective average concentration throughout the simulation, making it possible to systematically identify concentration effects on the dispersion. We define the concentration from the colloid volume fraction $\Phi = N_c \pi a^3/(6L_x L_y L_z)$, where $N_c$ is the total number of colloids in the system and $L_x$ is the effective channel width set by the atomistic walls (discussed in Sec. IV A). The numbers of colloid and solvent particles simulated for each concentration are summarized in Table I.

We equilibrated the suspensions for $10^5$ MD steps at rest and performed $5 \times 10^5$ MD steps to allow the flow to reach steady-state before performing measurements. We recorded the position and velocity of each colloid every 50 MD steps and conducted between 4 and 16 independent simulations for every colloid concentration and flow rate considered, each running at least $1.5 \times 10^8$ MD steps. We measured the mean squared displacement (MSD) of each colloid in the frame of reference of the average velocity of all colloids, $\langle (z - \overline{u}t)^2 \rangle$, because at long times the mean of the distribution advects with the average colloid velocity (see the Appendix). The dispersivity can be computed from the first derivative of the MSD with respect to time using Eq. (5). Figure 3 shows the results of this procedure for $\Phi = 0.005$ at increasing $g$, where the first derivative of the MSD has clearly converged to a limiting value. We determined $K$ by fitting over this plateau region. We emphasize the need to perform multiple independent simulations, particularly for dilute concentrations, over long times in order to obtain a reliable measurement of $K$.

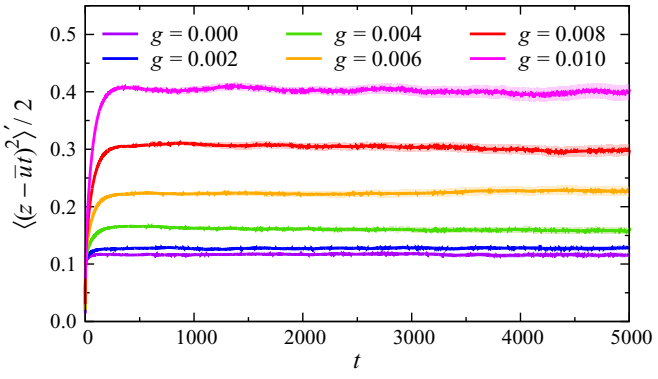


FIG. 3. Time derivative of the MSD along the flow direction of the channel for a dilute colloid suspension with $\Phi = 0.005$ at increasing $g$. The dark lines are averages over multiple independent simulations, while the shaded regions correspond to the measurement uncertainty determined from the standard error of the independent simulations (less than 2% of average values).

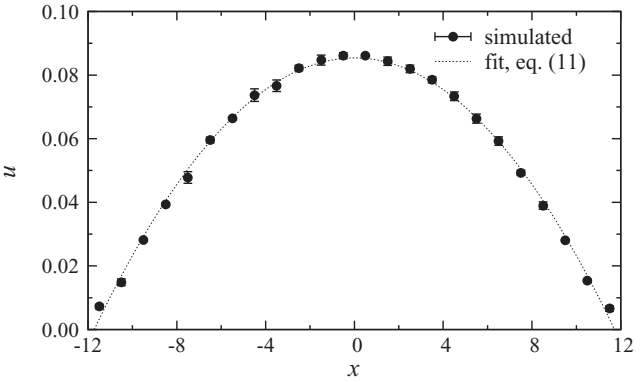


FIG. 4. Velocity profile of the pure solvent at $\rho_s = 0.62$, $T = 2.5$, and $g = 0.002$.

## IV. RESULTS AND DISCUSSION

The colloid distribution, velocity profile, and diffusion coefficients for our simulated model must be obtained to compare Eq. (6) against the direct simulation results. Ideally, these parameters could all be obtained theoretically so that predictions can be made independently of the simulations. In the present work, we estimate parameters for a dilute suspension of colloids with perfect slip because these are the conditions obtained in our simulations. In a physical system, the colloids are likely to have either no-slip or partial slip boundary conditions, which may modify the effective colloid velocity and the diffusion coefficients in confinement. These differences can be accommodated by appropriate modification of the theory presented here.

First, we characterize properties of our simulated system such as channel size, fluid properties, and colloid diameter. Then, we theoretically estimate the colloid distribution, flow profiles, and diffusion coefficients, and compare our predictions directly against the simulation results when possible. Finally, we incorporate these results into Eq. (6) to compare dispersion models of increasing detail with our simulation results.

### A. Model characterization

We investigated the flow behavior of the pure solvent in the parallel plate channel. We placed $N_s = 12873$ solvent particles randomly into the channel. We performed simulations for different acceleration constants, $0.002 \leqslant g \leqslant 0.010$, and measured the steady-state solvent velocity profile. Figure 4 shows a representative velocity profile of the pure solvent at $g = 0.002$, which clearly has the characteristic parabolic shape expected for pressure-driven flow of a Newtonian fluid between parallel plates

$$u(x) = \frac{3}{2}U\left[1 - \left(\frac{2x}{L_x}\right)^2\right], \tag{11}$$

where $U$ is the mean solvent velocity. We fit $U$ and $L_x$ to the simulated velocity profiles for the different flow rates, and found $L_x = 23.4 \pm 0.1$ independent of $g$, from which we compute an effective average solvent density of $\rho_s \approx 0.62$. The measured $L_x$ is slightly smaller than the nominal distance at which the walls were placed due to the roughness of the walls and the excluded volume between the solvent and wall particles. In order to determine the solvent viscosity, we used the relationship between $U$ and the fluid properties in this geometry,

$$U = \frac{\rho_s g L_x^2}{12\eta_s}, \tag{12}$$

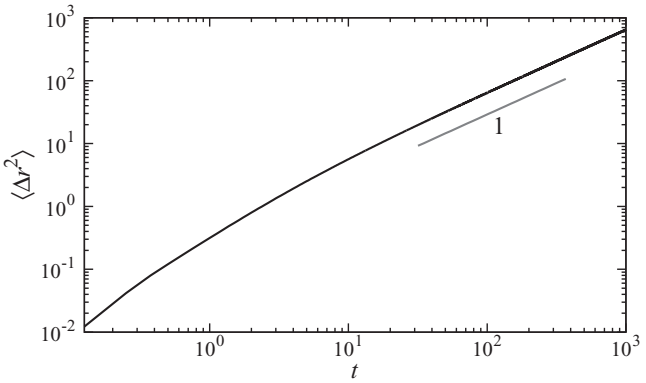


FIG. 5. Mean square displacement $\langle \Delta r^2 \rangle$ of a single colloid vs time $t$.

and found $\eta_s = 0.99 \pm 0.02$ in excellent agreement with the value of $1.00 \pm 0.03$ interpolated from available equilibrium data for the Lennard-Jones fluid [32,33].

In order to density match the colloid to the solvent, we needed to identify the effective colloid diameter $a$. We tentatively set the mass of the colloid using $a \approx \sigma_{cc}$ and $\rho_s = 0.62$. We then performed bulk simulations of a single colloid in a cubic simulation box of edge length $L = 20$ at the same effective density as in the parallel plate channel. In contrast to the suspensions in the parallel plate channels, isothermal conditions were achieved by applying a Nosé-Hoover thermostat to the suspension with time constant $\tau_{NH} = 0.5$. We measured the equilibrium diffusion coefficient of the colloid by computing its three-dimensional MSD, $\langle \Delta r^2 \rangle$, as a function of time. The simulated diffusion coefficient $D_L$ is related to the measured MSD by $\langle \Delta r^2 \rangle \sim 6 D_L t$ at sufficiently long times. We use the symbol $D_L$ to emphasize the fact that the diffusion coefficient measured in a simulation is system size dependent and needs to be corrected for finite-size effects, as explained later in this section. Figure 5 shows $\langle \Delta r^2 \rangle$ averaged from four independent runs. We can see that the motion of the colloid is ballistic at short times and then becomes fully diffusive after $t \gtrsim 30$, where the MSD achieves a slope of 1. We extracted a diffusion coefficient of $D_L = 0.107 \pm 0.005$ from this diffusive regime.

Due to the long-ranged nature of hydrodynamic interactions, the simulated $D_L$ must be corrected for finite-size effects of the periodic simulation box in order to obtain the true bulk diffusion coefficient $D$. We employed the correction derived by Yeh and Hummer [34]

$$D = D_L + \frac{\xi k_B T}{6\pi \eta L}, \tag{13}$$

where $\xi \approx 2.837297$ for a cubic simulation box and $\eta$ is the viscosity. We used $\eta \approx \eta_s$ for a single colloid, leading to a bulk diffusion coefficient $D = 0.126 \pm 0.005$. We verified the reliability of this correction by performing additional simulations in a simulation box with $L = 30$, and found $D_L = 0.114 \pm 0.004$ and $D = 0.127 \pm 0.004$.

For a single colloid, we also expect the diffusivity to be given by the Stokes-Einstein relation $D = \mu k_B T$, where $\mu$ is the mobility. Because the colloids are modeled as smooth spherical particles, the solvent is able to exert normal forces but no torques. Hence, we expect the colloids to have perfect slip boundary conditions, $\mu = 1/(2\pi \eta a)$. We can then estimate $a \approx 3.2$ using $\eta \approx \eta_s$. This estimate is consistent with our simulation model because the Lennard-Jones potential should exclude slightly more volume than the sphere defined by $\sigma_{ij}$ because the potential's minimum is at $2^{1/6}\sigma_{ij}$. Accordingly, we set the mass of our colloids to $m_c = 10.64$ in all simulations using $\rho_s = 0.62$.

We then additionally measured the bulk diffusion coefficient $D$ of our suspensions (edge length $L = 30$). $N_c$ and $N_s$ were appropriately adjusted for the larger volume of the simulation box compared to the slit channels. Because the suspension viscosity is not known *a priori*, we instead corrected our

data for finite-size effects of the periodic simulation box using the expression from Yeh and Hummer [34] for particles with slip boundary conditions that is independent of the suspension viscosity

$$D \approx D_L\left(1 - \frac{\xi a}{3L}\right)^{-1}. \tag{14}$$

The suspension diffusion coefficients reported in Table I decrease as a function of concentration. We qualitatively expect that this is due to an increase in the suspension viscosity. Cichocki and Felderhof [35] showed that the viscosity of dilute suspensions of colloids with slip boundary conditions is

$$\eta(\Phi) = \eta_s(1 + 2.5\Phi + 1.911\Phi^2), \tag{15}$$

which increases with concentration and can be considered a small correction of order $\Phi^2$ to the Einstein viscosity [36]. We repeated the correction of the measured suspension diffusion coefficients using Eq. (13) with the viscosity given by Eq. (15). We found quantitative agreement with the results obtained by Eq. (14), indicating that Eq. (15) is a reasonable constitutive equation for our simulated suspensions. We also compared $D$ with the values that would be predicted by the Stokes-Einstein relation for the suspension and found deviations of less than 4% over the range of concentrations we have considered.

### B. Colloid distributions

Colloidal mixtures of sufficiently high concentration adopt nonuniform density profiles in confinement. It is well known from classical statistical mechanics that this effect is present even for a simple purely repulsive hard sphere fluid against a structureless flat wall [5–7]. In this case, the fluid density is typically higher near the surface and decays to the bulk density far away. The structuring near the wall occurs only due to the excluded volume interactions both within the hard sphere fluid and against the wall, and to our knowledge has not been accounted for in previous theories of axial dispersion. We can incorporate this inhomogeneous particle distribution into our current model through an effective external potential $\phi$ that modifies the distribution $w$ according to Eq. (4).

Various statistical mechanical methods are available to predict the inhomogeneous density profiles of simple liquids [37]. In particular, classical density functional theories [38,39] and direct molecular simulations, e.g., Monte Carlo or MD, have been applied to predict the density profiles of fluids near surfaces [7,40,41] using only knowledge of the interparticle interactions. MD is obviously most expedient to determine the equilibrium particle distribution in the current work. However, we emphasize that this profile could also be determined theoretically by alternative computational methods or experimentally through appropriate particle tracking measurements.

The purely repulsive WCA colloids in our model can be approximately mapped onto the hard sphere fluid [24], and so are expected to exhibit similar structuring near the walls in confinement. Figure 6 shows the steady-state colloid distribution along the transverse direction, $w$, at increasing $\Phi$ both at rest and at $g = 0.010$. At the lowest concentration, $\Phi = 0.005$, the colloids are nearly uniformly distributed between the walls, but then gradually start to aggregate at the edges as $\Phi$ is increased.

Particles can undergo cross-stream inertial migration in Poiseuille flow [42], even at small but finite Reynolds number [43]. Inertial migration could lead to the focusing of particles onto planes near the walls in the parallel plate geometry, further enhancing the structuring observed in $w$. It has been shown that inertial migration effects are significant when the product of the particle Reynolds number, $\mathrm{Re}_c$, and particle Péclet number, $\mathrm{Pe}_c$, is greater than unity [12]. For our suspensions, we estimate $\mathrm{Re}_c \sim 0.4$ and $\mathrm{Pe}_c \sim 0.4$ using the definitions in Ref. [43], and so we expect that inertial effects should not be significant and any structuring should be due only to the colloid interactions in confinement. We confirmed this by repeating the measurement of $w$ under flow at $g = 0.010$ (the maximum flow rate considered) and found that the profiles are essentially indistinguishable. Accordingly, the

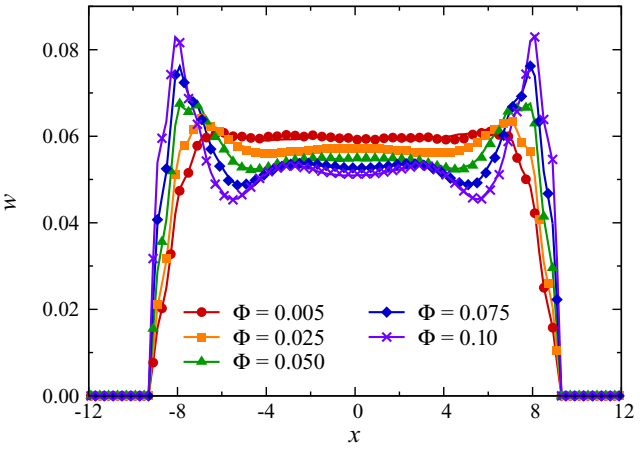


FIG. 6. Probability $w$ to find a colloid at a given $x$ position at rest (lines) and for $g = 0.010$ (symbols) for increasing colloid concentrations $\Phi$. Only every second point is drawn for $g = 0.010$. Error bars are omitted for clarity but are no larger than $\pm 10\%$ for all points.

equilibrium particle distribution may be applied even under flow for the concentrations and flow rates we have considered.

### C. Velocity profiles

At steady state, the colloid velocity profile should approximately satisfy the one-dimensional Navier-Stokes equation for gravity-driven flow

$$\frac{d}{dx}\left\{\eta[\Phi(x)]\frac{du}{dx}\right\} + \rho(x)g = 0 \tag{16}$$

with no-slip boundary conditions at the walls, $u(x = \pm L_x/2) = 0$. We neglect any additional flows between the colloids and the walls, and any lag in the colloid velocity relative to the solvent. Here, $\rho(x)$ is the density of the suspension with contributions due to the solvent and the colloids, which may in principle depend on transverse position due to the confinement. Because the colloids are density matched to the solvent, we can approximate the total suspension density as a uniform distribution

$$\rho(x) \approx \rho = \frac{m_s N_s + m_c N_c}{L_x L_y L_z}. \tag{17}$$

The suspension viscosity $\eta$ is a function of concentration, which depends on the colloid volume distribution. The colloid volume distribution can be computed by convolving $w$, which effectively gives the distribution of the colloid center of mass, with the volume of a colloid in three dimensions,

$$\Phi(x) = \frac{N_c}{L_y L_z}\int w(x - x')\Theta(a/2 - |\mathbf{r}'|)d\mathbf{r}', \tag{18}$$

where $x'$ is the $x$ component of $\mathbf{r}'$, $|\mathbf{r}'|$ is the magnitude of $\mathbf{r}'$, and $\Theta$ is the Heaviside step function. The resulting distributions for $\Phi(x)$ are qualitatively similar to $w$, but are slightly smoothed near the channel walls.

We solved Eq. (16) numerically using Eq. (18) for $\Phi(x)$ with Eq. (15) for $\eta$. We emphasize that there are no free parameters used when solving Eq. (16). Figure 7 compares the steady-state colloid velocity profiles measured from flow simulations at $g = 0.010$ with the numerical solution. In all cases, the maximum velocities predicted by the numerical solution are in excellent agreement with the simulated data. At the highest concentrations, the curvature of the simulated velocity profiles

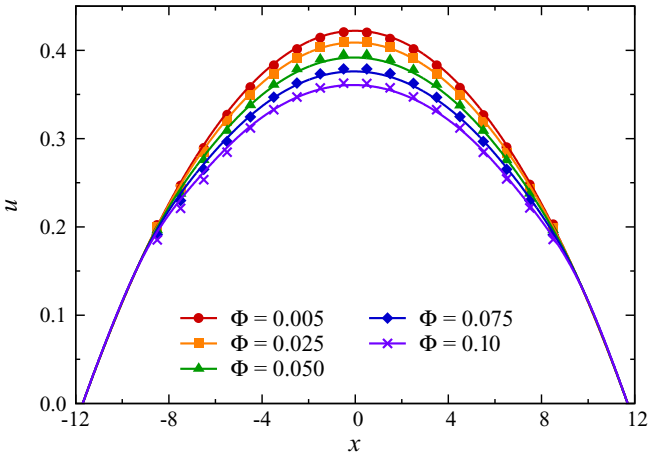


FIG. 7. Suspension velocity profiles $u$ at $g = 0.010$ for increasing colloid concentrations $\Phi$. Symbols are measured from simulations, and lines are calculated from Eq. (16). Error bars for the simulated data are smaller than the symbol size.

is somewhat steeper than predicted by Eq. (16). This deviation in the near-wall region may be partially due to colloid-wall hydrodynamic interactions, which may reduce the colloid velocity. We will assess the importance of these deviations for computing the dispersion coefficient in Sec. IV E. We did not observe any lag between the colloid velocity and that of the solvent in our simulations [1], consistent with numerical and experimental results for neutrally buoyant spherical particles of comparably sized particles in a parallel plate channel [44,45].

In the limit that the colloids explore the channel uniformly, the velocity profile given by Eqs. (16) and (18) should be essentially parabolic. However, it is evident that the velocity profiles in Fig. 7 are not parabolic due to the spatially varying viscosity of the suspension. Hence, it is important to consider the effects of confinement on the velocity profile when the density profile is highly nonuniform or when there are strong repulsions between the colloids and the channel walls that exclude the colloid from accessing significant regions of the channel.

### D. Diffusion coefficients

Considerable theoretical effort has been undertaken to predict the diffusion coefficient of bulk colloidal suspensions [35,46,47]. Incorporating the effects of confinement on the suspension is an even greater theoretical challenge. In the present work, we approximate the diffusion coefficient in confinement from results for the Stokes flow of a single colloid. Wacholder and Weihs exactly solved the enhancement to the drag on a spherical fluid droplet moving perpendicular to a single planar wall [48], which affects the observed transverse diffusion coefficient $D_x$. From their work, the mobility of a spherical particle with perfect slip boundary conditions is reduced by a factor $1/\lambda_1$, where

$$\lambda_1(d) = \sinh\alpha \sum_{n=1}^{\infty} \frac{n(n+1)}{(2n-1)(2n+3)} \left[ \frac{(2n+3)e^{2\alpha} + 4e^{-(2n+1)\alpha} - (2n-1)e^{-2\alpha}}{2\sinh(2n+1)\alpha - (2n+1)\sinh 2\alpha} \right], \tag{19}$$

$d$ is the center-of-mass separation from the wall, and $\alpha = \cosh^{-1}(2d/a)$. In the limit of large separations, the unperturbed mobility is recovered. Using the method of reflections [49–51], Eq. (19) can be used to approximate the drag on a particle in a channel by superimposing the effects of two walls at $x = 0$ and $x = L_x$. The particle mobility at center-of-mass position $x$ is reduced by $1/\lambda_2$, where

$$\lambda_2(x) \approx \lambda_1(x) + \lambda_1(L_x - x) - 1. \tag{20}$$

The transverse diffusion coefficient of the confined suspension is then approximately related to the bulk diffusion coefficient by $D_x(x;\Phi) \approx D(\Phi)/\lambda_2(x)$. $D$ can be determined by measurement or an appropriate theoretical model. In this work, we will use the measured bulk diffusion coefficients of Table I, which are in good agreement with Stokes-Einstein predictions.

Chang and Keh have used a semianalytical boundary colocation method to exactly solve the drag on a spherical fluid droplet moving perpendicular to two planar walls [52]. Equation (20) overestimates the drag they reported for a particle with perfect slip boundary conditions on the centerline by about 5%. However, their solution is considerably more computationally demanding to evaluate than Eq. (19). Moreover, we have already made a more significant approximation that the result for a single particle can be applied to the suspension of many particles. In reality, there are additional flows (reflections) between particles that may incur error at higher particle concentrations.

We attempted to validate Eq. (20), but found that it was challenging to measure $D_x$ directly in our simulations. We observed in the bulk that a colloid translated a significant fraction of the accessible channel width before it entered the diffusive regime (see Fig. 5). During this time, the particle is not a purely Brownian walker, and so standard techniques for evaluating the diffusion coefficient are unsuitable. We accept Eq. (20) as a reasonable approximation for lack of an alternative theory for the simultaneous effects of confinement and concentration on diffusion of a suspension, and will later validate its usefulness from the axial dispersion measurements.

The axial diffusion coefficient $\overline{D}_z$ should also be affected by confinement to some extent [52,53]. However, the periodic boundary conditions of our simulation box may also affect the observed diffusion, as they do in the bulk, making it challenging to theoretically predict this quantity for the simulated system. Since $\overline{D}_z$ amounts only to a constant offset in the overall dispersivity and can be determined experimentally by appropriate extrapolation of $K$ as $g$ tends to zero, we simply measure the effective diffusion coefficient $\overline{D}_z$ for the suspension at rest (see, for example, $g = 0.000$ in Fig. 3), and report the diffusivity in Table I. Typically, $\overline{D}_z$ is roughly 85% to 90% of $D$ for our suspensions. If it is not possible to determine $\overline{D}_z$, a theoretical prediction can be obtained in a manner analogous to Eqs. (19) and (20) for motion parallel to a planar surface (see, for example, Ref. [53]).

### E. Axial dispersion

The results derived so far can be applied in Eq. (6) to develop models of increasing detail for the axial dispersion. We start from the classical Taylor-Aris case in the parallel plate channel, in which point particles access the entire channel uniformly so $\ell = L_x$ and $w(x) = 1/L_x$. The classical parabolic velocity profile of Eq. (11) is assumed. The diffusion coefficients are taken to be isotropic so that $D_x = D_z = D$. Taking the integrals in Eqs. (6) and (8) gives the well-known result [54]

$$K/D = 1 + \frac{\mathrm{Pe}^2}{210}, \tag{21}$$

where the Péclet number is defined as $\mathrm{Pe} = UL_x/D$.

Using geometric considerations, James and Chrysikopoulos [11] derived an expression for the dispersivity of rigid colloids between parallel plates when the colloids are excluded from part of the channel but otherwise remain uniformly distributed. The assumptions related to the velocity profile and isotropic diffusion remain unchanged. The dispersivity is then

$$K/D = 1 + \frac{\mathrm{Pe}^2}{210}\left(\frac{\ell}{L_x}\right)^6. \tag{22}$$

We can relax the assumption of isotropic diffusion in Eq. (22) by replacing the transverse diffusion coefficient by its average value in the accessible channel width, $\overline{D}_x$. This assumption is reasonable when the variations in $D_x$ across the accessible channel width are not too large. From this, we

TABLE II. Theoretical models for axial dispersion.

| Model | Ref. | Eq. | Parameters |
|---|---|---|---|
| A | [54] | (21) | $D = \overline{D}_z$ |
| B | [11] | (22) | $D = \overline{D}_z$, $\ell = 18.2$ |
| C | This work | (23) | $D_x = \overline{D}_x$, $\ell = 18.2$ |
| D | This work | (6) | $D_x = D_x(x)$, $w(x)$ from Fig. 6 |

analogously obtain

$$K/\overline{D}_z = 1 + \frac{\overline{\mathrm{Pe}}^2}{210}\left(\frac{\ell}{L_x}\right)^6, \tag{23}$$

where $\overline{\mathrm{Pe}} = UL_x/(\overline{D}_x\overline{D}_z)^{1/2}$. We expect that these approximate models should be less accurate than the full prediction of Eq. (6).

Table II summarizes the equations and parametrizations used in these models in order to make direct comparison with simulation data. Model A is the classical Taylor-Aris result for the parallel plate channel, in which we set $D = \overline{D}_z$ so that $K/\overline{D}_z = 1$ at rest. Model B incorporates the effects of the accessible channel width to model A, but still assumes isotropic diffusion. Model C adds anisotropic diffusion through Eq. (23). Finally, model D fully incorporates the nonuniform colloid distribution into Eq. (6) through $w$ and $u$, and so includes all the parameters and effects considered so far in this work. In models A, B, and C, the characteristic velocity $U$ is calculated using Eq. (11) with the suspension density and viscosity. In models B and C, we set the accessible width $\ell \approx 18.2$, estimated from the accessible region shown in Fig. 6 and the expected range of the repulsive wall potential acting on the colloids. We obtain $\overline{D}_x$ for model C by taking an average of $D(x)$ with the uniform distribution so that $\overline{D}_x \approx 0.75D$.

All models, including model D, predict enhancements that increase quadratically with the acceleration constant $g$ because $K \sim U^2$ in Eq. (6) and $U \sim g$ from Eq. (16). Figure 8 compares the theoretical predictions of the different models to the simulated enhancements $K/\overline{D}_z$ as a function of $g$ for the most dilute concentration, $\Phi = 0.005$. At this concentration, the colloids are nearly uniformly distributed in the channel, and so models B and C are expected to perform their best at these conditions. It is apparent that model A vastly overpredicts the enhancement. This should not be surprising, based on the strong dependence of Eqs. (22) and (23) on the accessible channel width,

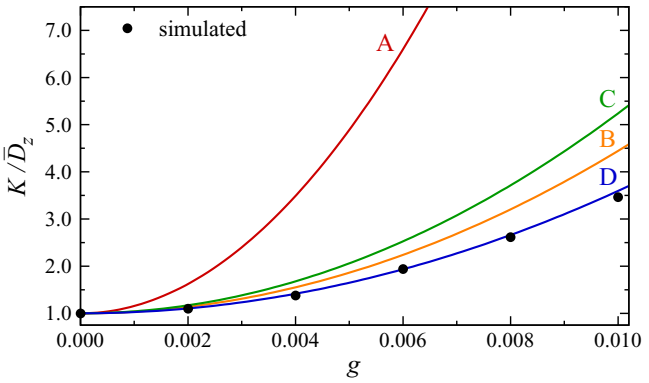


FIG. 8. Comparison of predictions of different models for the enhancement of the axial diffusion, $K/\overline{D}_z$, as a function of acceleration constant $g$ at $\Phi = 0.005$. Model predictions are given by labeled curves, while the simulated values are plotted as points. Error bars for the simulated values are smaller than the symbol size. See Table II for model details.

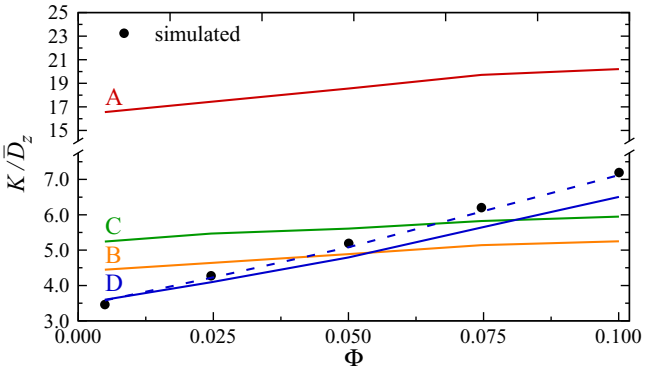


FIG. 9. Comparison of predictions of different models for the enhancement of the axial diffusion, $K/\overline{D}_z$, as a function of concentration $\Phi$ at fixed $g = 0.010$. Model predictions are given by labeled curves, while the simulated values are plotted as points. Error bars for the simulated data are smaller than the symbol size. The dashed line corresponds to prediction of model D with the velocity profiles from Eq. (16) replaced by the simulated velocity profiles of Fig. 7.

which predict an ≈80% reduction in the dispersivity due to the exclusion of the colloid from the slowest parts of the velocity profile. The remaining models are quantitatively much closer to the simulated enhancements. Model C differs from model B by a factor of $\overline{D}_z/\overline{D}_x$, which is typically greater than 1 for our simulated suspensions (and more generally for a single particle between two parallel plates), and so model C consistently predicts a larger enhancement than model B. For the dilute case, model D gives the best quantitative prediction of the dispersion.

In order to assess which model performs best across multiple concentrations, we compare the predicted relative enhancements as a function of increasing concentration at fixed $g = 0.010$, shown in Fig. 9. Model A clearly overpredicts the relative enhancement for all concentrations by a large factor. This overprediction is in agreement with the numerical results of Sané *et al.* [23]. The predictions of models B and C are much closer to the simulated enhancements, but fail at capturing the correct concentration dependence of $K/\overline{D}_z$. Only model D is able to produce reasonable agreement between the theory and simulation data for the entire concentration range.

Although model D captures the qualitative concentration dependence of $K/\overline{D}_z$ best from the four models considered, it consistently underpredicts the dispersion by a small amount at the highest concentrations. We attribute this error to the incorrect curvature of the velocity profiles predicted by Eq. (16) at the higher concentrations in the near-wall regions. Qualitatively, we expect that the dispersion should increase if the velocity gradient is steeper because the colloids advect faster relative to the mean. This error is further amplified at the higher concentrations because the colloid distribution is biased towards the wall region, where the error in the velocity is largest. We confirmed this source of error by recomputing the dispersion coefficient using model D with the velocity profiles from the simulations. The predicted enhancement is shown as a dashed line in Fig. 9 and is in quantitative agreement with the simulated data. This indicates the sensitivity of the dispersion prediction to small errors in the velocity, especially near the channel walls, and the importance of reliably predicting the colloid velocity profile.

Although not shown in Fig. 9, we also replaced $D_x = \overline{D}_x$ in model D, and observed only a negligible difference in the predicted enhancements. Hence, the most significant difference between models C and D is the colloid distribution. We conclude that the colloid distribution is the most significant factor controlling the concentration dependence of the enhanced dispersion. This makes physical sense given that the colloid distribution controls how the colloid explores the streamlines of the velocity profile that drive dispersion.

Consider two extreme cases. There is no enhancement to the dispersion when the colloid is confined to a single streamline because it always advects with its mean velocity. In the opposite

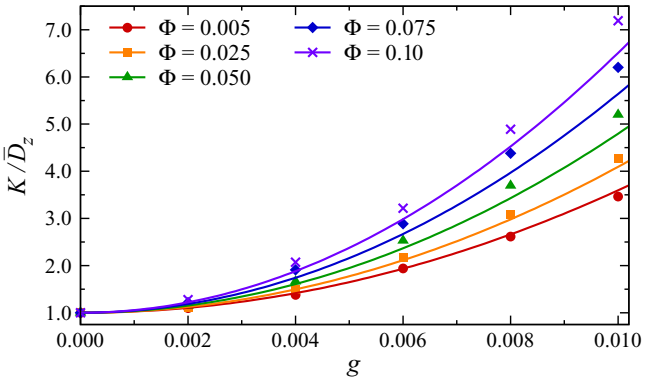


FIG. 10. Enhancement of the axial dispersion, $K/\overline{D}_z$, as a function of applied body force per mass $g$ for colloidal suspensions of increasing concentration $\Phi$. Symbols are simulation results, while lines are predictions from model D. Error bars for the simulated data are smaller than the symbol size.

case, the enhancement is maximized if the particle is distributed in such a way that it spends half its time advecting at the maximum possible velocity, and the other half advecting at the slowest possible velocity. As concentration increases, peaks are obtained towards the extrema regions of the velocity profile. It is then crucial to obtain a reliable estimate for the distribution of the particles in the channel.

Figure 10 concisely highlights the results of the present work by comparing the simulated enhancement of the axial dispersion to the predictions of model D for all five concentrations considered as a function of flow rate. The agreement between the simulations and the predictions is good in all cases and can be made completely quantitative by correcting for the simulated velocity profile (not shown here). The enhancement increases monotonically as a function of $\Phi$. From Eq. (6), the enhancement qualitatively scales with the Péclet number, $K/D \sim (UL/D)^2$, but $U$ and $D$ should both scale in the same way with concentration due to their inverse dependence on the viscosity. Hence, we attribute the increase in the relative enhancement as a function of concentration to the increasingly nonuniform colloid distribution, which biases the colloids to the streamlines that have the largest deviation from the mean velocity and controls the exact scaling prefactor.

Ultimately, however, all the effects of confinement on the colloid distribution and diffusion are relevant. Although the qualitative concentration dependence of model C is not significantly different from model B, there is a considerable quantitative difference due only to the anisotropic diffusion. Indeed, model D would also fail to quantitatively predict the dispersion if the bulk diffusion coefficient were used rather than $D_x$. The fact that $D_x$ could be reasonably replaced by $\overline{D}_x$ in model D suggests that Eq. (20) provides a reasonably estimate of $\overline{D}_x$, but the exact functional form for $D_x$ is not necessary. This is promising for experiments seeking to *determine* the transverse diffusion coefficient by fitting dispersion data rather than make predictions.

## V. CONCLUSIONS

We developed a predictive model for the axial dispersion of Brownian colloids in confinement. We showed that nonuniform colloid distributions that arise in confinement due solely to interparticle interactions significantly influenced the effective axial dispersion. The axial dispersion was also found to be sensitive to the colloid velocity profile near the channel walls and the anisotropic diffusion tensor. Our model gave good predictions for the flow rate and concentration dependence of the dispersion coefficients measured from explicit molecular dynamics simulations that fully take into account hydrodynamic correlations and thermal fluctuations. This model should prove useful in many

applications involving the axial dispersion of colloids, including extracting diffusion coefficients from microfluidic experiments and modeling the transport of colloids in geological fractures.

In this article, we have restricted ourselves to analyzing dilute suspensions of Brownian colloids with slip boundary conditions. The presented theoretical framework can be easily extended to no-slip or partial slip boundary conditions on the colloids by appropriate modification of the expressions for the colloid velocity and diffusion coefficients. At high concentrations, the mean-field approximation that the motion of individual colloids is independent may break down due to correlations between particles. Moreover, at high concentrations or flow rates, shearing between colloids may cause the effective diffusion coefficients to have an additional flow-rate dependence. The approximations for the colloid velocity profile and diffusion coefficients may become less accurate for sufficiently large particle diameters relative to the channel width due to increased colloid-wall interactions. Unfortunately, the employed simulation approach is not suitable to access these conditions due to two challenges: (1) diffusion slows considerably as concentration or particle diameter increases and it becomes difficult to reliably measure the dispersion and (2) more heat is generated at high flow rates than can be reasonably removed through the channel walls alone and thermal gradients develop. These difficulties might be overcome with a mesoscale simulation approach to determine the concentrations and particle sizes at which deviations from the presented theory are observed.

## ACKNOWLEDGMENTS

We thank H. A. Stone for suggesting the Taylor dispersion problem to us and for many fruitful discussions. M.P.H. received Government support under Contract No. FA9550-11-C0028 and awarded by the Department of Defense, Air Force Office of Scientific Research, National Defense Science and Engineering Graduate (NDSEG) Fellowship, 32 CFR 168a. A.N. acknowledges funding from the German Research Foundation (DFG) under the Project No. NI 1487/2-1. Additional financial support for this work was provided by the Princeton Center for Complex Materials (PCCM), a US National Science Foundation Materials Research Science and Engineering Center (Grant No. DMR-1420541). The authors gratefully acknowledge the computing time granted on the supercomputer Mogon at Johannes Gutenberg University Mainz (www.hpc.uni-mainz.de).

## APPENDIX: MOMENT ANALYSIS

Our derivation is adapted from that of Brenner and Gaydos in a cylindrical tube [9], and accordingly we present it in similar form and notation to allow the interested reader to compare. We define axial moments $\mu_m$ and total moments $M_m$ of the distribution

$$\mu_m = \int_{-\infty}^{\infty} (z - z_0)^m p dz, \quad M_m = \int_{-\ell/2}^{\ell/2} \mu_m dx, \tag{A1}$$

and assume that $(z - z_0)^m p \to 0$ as $z \to \pm\infty$ in order that $\mu_m$ remains finite. By the normalization condition on $p$, $M_0 = 1$. Using Eq. (5), the dispersivity can be computed from the total moments

$$K = \frac{1}{2} \lim_{t\to\infty} \left[ \frac{dM_2}{dt} - 2M_1 \frac{dM_1}{dt} \right]. \tag{A2}$$

The problem then reduces to computing the first and second moments of the distribution. Taking the axial moments of Eq. (3) and integrating by parts gives

$$\frac{\partial \mu_m}{\partial t} = \mathcal{L}[\mu_m] + mu(x)\mu_{m-1} + m(m-1)D_z(x)\mu_{m-2}, \tag{A3}$$

where $\mathcal{L}$ is a compact notation for the operator

$$\mathcal{L}[p] = \frac{\partial}{\partial x} \left\{ w(x) D_x(x) \frac{\partial}{\partial x} \left[ \frac{p}{w(x)} \right] \right\}. \tag{A4}$$

Explicitly, the first three moments are

$$\frac{\partial \mu_0}{\partial t} = \mathcal{L}[\mu_0], \tag{A5}$$

$$\frac{\partial \mu_1}{\partial t} = \mathcal{L}[\mu_1] + u(x)\mu_0, \tag{A6}$$

$$\frac{\partial \mu_2}{\partial t} = \mathcal{L}[\mu_2] + 2u(x)\mu_1 + 2D_z(x)\mu_0. \tag{A7}$$

The transformed no-flux boundary conditions at $x = \pm\ell/2$ are

$$\mathbf{j}_{x,m} = -w(x)D_x(x)\frac{\partial}{\partial x}\left[\frac{\mu_m}{w(x)}\right] = 0. \tag{A8}$$

The transformed initial conditions are $\mu_0(x,t=0) = \delta(x - x_0)$ and $\mu_m(x,t=0) = 0$ for $m > 0$.

We begin by solving for $\mu_0$, which is essentially the marginal distribution of the colloid along the transverse channel dimension. The steady-state solution that satisfies the normalization condition is $w(x)$, or equivalently, the Boltzmann distribution in the external field. This moment is expected to relax exponentially to its steady state. Since we are interested in long-time behavior, we neglect these transient terms and adopt a quasisteady state approximation for $\mu_0(x,t) \approx w(x)$. This approximation is valid after a characteristic diffusion time $\tau \sim \ell^2/\overline{D}_x$. Note that using this approximation it is no longer possible to satisfy the initial condition.

We substitute $\mu_0$ into Eq. (A6) and guess a solution of the form

$$\mu_1 \sim w(x)[\overline{u}t + B(x)] \tag{A9}$$

so that

$$\frac{d}{dx}\left[w(x)D_x(x)\frac{dB}{dx}\right] = -(u - \overline{u})w(x). \tag{A10}$$

At the boundaries, $-w(x)D_x(x)dB/dx = 0$, so integrating across the channel yields Eq. (8), and demonstrates that $\overline{u}$ is precisely the average velocity of the colloid. Integrating twice allows us to evaluate $B(x)$

$$B(x) = B(-\ell/2) - \int_{-\ell/2}^{x} \frac{dx'}{w(x')D_x(x')} \int_{-\ell/2}^{x'} [u(\hat{x}) - \overline{u}]w(\hat{x})d\hat{x}. \tag{A11}$$

The existence of such a solution validates the original guess for the functional form. The first total moment is

$$M_1(t) \approx \overline{u}t + C, \tag{A12}$$

where we defined the constant $C$ for convenience

$$C \equiv \int_{-\ell/2}^{\ell/2} B(x)w(x)dx. \tag{A13}$$

The time derivative $\mathrm{d}M_1/\mathrm{d}t \approx \overline{u}$, showing that the mean of the distribution advects with the mean colloid velocity, as it should. For the second (and higher) order moment(s),

$$\frac{dM_m}{dt} = \int_{-\ell/2}^{\ell/2} \frac{\partial \mu_m}{\partial t} dx \tag{A14}$$

$$= m\int_{-\ell/2}^{\ell/2} u(x)\mu_{m-1}dx + m(m-1)\int_{-\ell/2}^{\ell/2} D_z(x)\mu_{m-2}dx, \tag{A15}$$

which is obtained by substituting Eq. (A3) and applying the boundary conditions on $\mu_m$. For $m = 2$, substituting $\mu_0$ and $\mu_1$ and simplifying gives

$$\frac{dM_2}{dt} = 2\left[\overline{u}^2 t + \int_{-\ell/2}^{\ell/2} u(x)w(x)B(x)dx + \overline{D}_z\right], \tag{A16}$$

where $\overline{D}_z$ is defined by Eq. (7). Multiplying Eq. (A10) by $B(x)$ and integrating by parts allows us to evaluate the integral to give

$$\frac{dM_2}{dt} \approx 2\overline{u}^2 t + 2\overline{u}C + 2\overline{D}_z + 2\int_{-\ell/2}^{\ell/2} \frac{dx}{w(x)D_x(x)}\left\{\int_{-\ell/2}^{x} [u(\hat{x}) - \overline{u}]w(\hat{x})d\hat{x}\right\}^2. \tag{A17}$$

Substituting Eqs. (A12) and (A17) into Eq. (A2) gives Eq. (6).

---


[1] H. Brenner and D. A. Edwards, *Macrotransport Processes* (Butterworth-Heinemann, Boston, MA, 1993).

[2] G. Taylor, Dispersion of soluble matter in solvent flowing slowly through a tube, Proc. R. Soc. A **219**, 186 (1953).

[3] G. Taylor, Conditions under which dispersion of a solute in a stream of solvent can be used to measure molecular diffusion, Proc. R. Soc. London, Ser. A **225**, 473 (1954).

[4] R. Aris, On the dispersion of a solute in a fluid flowing through a tube, Proc. R. Soc. London, Ser. A **235**, 67 (1956).

[5] J. W. Perram and L. R. White, Structure of the liquid/vapour and liquid/solid interfaces, Faraday Discuss. Chem. Soc. **59**, 29 (1975).

[6] D. Henderson, F. F. Abraham, and J. A. Barker, The Ornstein-Zernike equation for a fluid in contact with a surface, Mol. Phys. **31**, 1291 (1976).

[7] I. K. Snook and D. Henderson, Monte Carlo study of a hard-sphere fluid near a hard wall, J. Chem. Phys. **68**, 2134 (1978).

[8] H. Brenner, Effect of finite boundaries on the Stokes resistance of an arbitrary particle, J. Fluid Mech. **12**, 35 (1962).

[9] H. Brenner and L. J. Gaydos, The constrained Brownian movement of spherical particles in cylindrical pores of comparable radius: Models of the diffusive and convective transport of solution molecules in membranes and porous media, J. Colloid Interface Sci. **58**, 312 (1977).

[10] C. A. Silebi and J. G. DosRamos, Axial dispersion of submicron particles in capillary hydrodynamic fractionation, AIChE J. **35**, 1351 (1989).

[11] S. C. James and C. V. Chrysikopoulos, Effective velocity and effective dispersion coefficient for finite-sized particles flowing in a uniform fracture, J. Colloid Interface Sci. **263**, 288 (2003).

[12] S. Bhattacharya, D. K. Gurung, and S. Navardi, Radial distribution and axial dispersion of suspended particles inside a narrow cylinder due to mildly inertial flow, Phys. Fluids **25**, 033304 (2013).

[13] I. M. Griffiths and H. A. Stone, Axial dispersion via shear-enhanced diffusion in colloidal suspensions, Europhys. Lett. **97**, 58005 (2012).

[14] H. A. Stone, A. D. Stroock, and A. Ajdari, Engineering flows in small devices: Microfluidics toward a lab-on-a-chip, Annu. Rev. Fluid Mech. **36**, 381 (2004).

[15] A. Ajdari, N. Bontoux, and H. A. Stone, Hydrodynamic dispersion in shallow microchannels: The effect of cross-sectional shape, Anal. Chem. **78**, 387 (2006).

[16] N. Bontoux, A. Pépin, Y. Chen, A. Ajdari, and H. A. Stone, Experimental characterization of hydrodynamic dispersion in shallow microchannels, Lab Chip **6**, 930 (2006).

[17] C. C. Hong, J. W. Choi, and C. H. Ahn, A novel in-plane passive microfluidic mixer with modified Tesla structures, Lab Chip **4**, 109 (2004).

[18] T. M. Squires and S. R. Quake, Microfluidics: Fluid physics at the nanoliter scale, Rev. Mod. Phys. **77**, 977 (2005).
[19] C. S. Garbe, K. Roetmann, V. Beushausen, and B. Jähne, An optical flow MTV based technique for measuring microfluidic flow in the presence of diffusion and Taylor dispersion, Exp. Fluids **44**, 439 (2008).
[20] B. M. Belongia and J. C. Baygents, Measurements on the diffusion coefficient of colloidal particles by Taylor-Aris dispersion, J. Colloid Interface Sci. **195**, 19 (1997).
[21] F. d'Orlyé, A. Varenne, and P. Gareil, Determination of nanoparticle diffusion coefficients by Taylor dispersion analysis using a capillary electrophoresis instrument, J. Chromatogr. A **1204**, 226 (2008).
[22] E. O. Fridjonsson, J. D. Seymour, and S. L. Codd, Anomalous preasymptotic colloid transport by hydrodynamic dispersion in microfluidic capillary flow, Phys. Rev. E **90**, 010301(R) (2014).
[23] J. Sané, J. T. Padding, and A. A. Louis, Taylor dispersion of colloidal particles in narrow channels, Mol. Phys. **113**, 2538 (2015).
[24] J. D. Weeks, D. Chandler, and H. C. Andersen, Role of repulsive forces in determining the equilibrium structure of simple liquids, J. Chem. Phys. **54**, 5237 (1971).
[25] R. Khare, J. J. de Pablo, and A. Yethiraj, Rheology of confined polymer melts, Macromolecules **29**, 7910 (1996).
[26] R. Khare, J. de Pablo, and A. Yethiraj, Molecular simulation and continuum mechanics study of simple fluids in non-isothermal planar couette flows, J. Chem. Phys. **107**, 2589 (1997).
[27] W. Humphrey, A. Dalke, and K. Schulten, VMD: Visual molecular dynamics, J. Mol. Graphics **14**, 33 (1996).
[28] J. A. Anderson, C. D. Lorenz, and A. Travesset, General purpose molecular dynamics simulations fully implemented on graphics processing units, J. Comput. Phys. **227**, 5342 (2008).
[29] J. Glaser, T. D. Nguyen, J. A. Anderson, P. Lui, F. Spiga, J. A. Millan, D. C. Morse, and S. C. Glotzer, Strong scaling of general-purpose molecular dynamics simulations on GPUs, Comput. Phys. Commun. **192**, 97 (2015).
[30] http://codeblue.umich.edu/hoomd-blue
[31] M. P. Howard, J. A. Anderson, A. Nikoubashman, S. C. Glotzer, and A. Z. Panagiotopoulos, Efficient neighbor list calculation for molecular simulation of colloidal systems using graphics processing units, Comput. Phys. Commun. **203**, 45 (2016).
[32] R. L. Rowley and M. M. Painter, Diffusion and viscosity equations of state for a Lennard-Jones fluid obtained from molecular dynamics simulations, Int. J. Thermophys. **18**, 1109 (1997).
[33] K. Meier, A. Laesecke, and S. Kabelac, Transport coefficients of the Lennard-Jones model fluid, I. Viscosity, J. Chem. Phys. **121**, 3671 (2004).
[34] I.-C. Yeh and G. Hummer, System-size dependence of diffusion coefficients and viscosities from molecular dynamics simulations with periodic boundary conditions, J. Phys. Chem. B **108**, 15873 (2004).
[35] B. Cichocki and B. U. Felderhof, Long-time self-diffusion coefficient and zero-frequency viscosity of dilute suspensions of spherical Brownian particles, J. Chem. Phys. **89**, 3705 (1988).
[36] A. Einstein, Eine neue Bestimmung der Moleküldimensionen, Ann. Phys. (Berlin, Germany) **324**, 289 (1906); Berichtigung zu meiner Arbeit: Eine neue Bestimmung der Moleküldimensionen, *ibid.* **339**, 591 (1911).
[37] R. Evans, The nature of the liquid-vapour interface and other topics in the statistical mechanics of non-uniform, classical fluids, Adv. Phys. **28**, 143 (1979).
[38] P. Tarazona, J. A. Cuesta, and Y. Martínez-Ratón, Density functional theories of hard particle systems, in *Theory and Simulation of Hard-Sphere Fluids and Related Systems*, edited by Ángel Mulero (Springer, Berlin, 2008), Chap. 7, p. 247.
[39] R. Roth, Fundamental measure theory for hard-sphere mixtures: A review, J. Phys. Condens. Matter **22**, 063102 (2010).
[40] P. C. Ball and R. Evans, The density profile of a confined fluid: Comparison of density functional theory and simulation, Mol. Phys. **63**, 159 (1988).
[41] S. Sokolowski and J. Fischer, Lennard-Jones mixtures in slit-like pores: A comparison of simulation and density-functional theory, Mol. Phys. **71**, 393 (1990).

[42] G. Segré and A. Silberberg, Radial particle displacements in Poiseuille flow of suspensions, Nature (London) **189**, 209 (1961).
[43] S. Bhattacharya, D. K. Gurung, and S. Navardi, Radial lift on a suspended finite-sized sphere due to fluid inertia for low-Reynolds-number flow through a cylinder, J. Fluid Mech. **722**, 159 (2013).
[44] M. E. Staben, A. Z. Zinchenko, and R. H. Davis, Motion of a particle between two parallel plane walls in low-Reynolds-number Poiseuille flow, Phys. Fluids **15**, 1711 (2003) [Erratum: **16**, 4206 (2004)].
[45] M. Staben and R. Davis, Particle transport in poiseuille flow in narrow channels, Int. J. Multiphase Flow **31**, 529 (2005).
[46] J. F. Brady, The long-time self-diffusivity in concentrated colloidal dispersions, J. Fluid Mech. **272**, 109 (1994).
[47] A. Imhof, A. van Blaaderen, G. Maret, J. Mellema, and J. K. G. Dhont, A comparison between the long-time self-diffusion and low shear viscosity of concentrated dispersions of charged colloidal silica spheres, J. Chem. Phys. **100**, 2170 (1994).
[48] E. Wacholder and D. Weihs, Slow motion of a fluid sphere in the vicinity of another sphere or a plane boundary, Chem. Eng. Sci. **27**, 1817 (1972).
[49] J. Happel and H. Brenner, Low Reynolds number hydrodynamics, in *Mechanics of Fluids and Transport Processes* (Martinus Nijohff, Boston, 1983).
[50] L. Lobry and N. Ostrowsky, Diffusion of Brownian particles trapped between two walls: Theory and dynamic-light-scattering measurements, Phys. Rev. B **53**, 12050 (1996).
[51] B. H. Lin, J. Yu, and S. A. Rice, Direct measurements of constrained Brownian motion of an isolated sphere between two walls, Phys. Rev. E **62**, 3909 (2000).
[52] Y. C. Chang and H. J. Keh, Slow motion of a slip spherical particle perpendicular to two plane walls, J. Fluid Struct. **22**, 647 (2006).
[53] H. J. Keh and P. Y. Chen, Slow motion of a droplet between two parallel plane walls, Chem. Eng. Sci. **56**, 6863 (2001).
[54] R. A. Wooding, Instability of a viscous liquid of variable density in a vertical Hele-Shaw cell, J. Fluid Mech. **7**, 501 (1960).